



From rock to magma and back again: The evolution of temperature and deformation mechanism in conduit margin zones



Michael J. Heap^{a,*}, Marie Violay^b, Fabian B. Wadsworth^c, Jérémie Vasseur^c

^a Géophysique Expérimentale, Institut de Physique de Globe de Strasbourg (UMR 7516 CNRS, Université de Strasbourg/EOST), 5 rue René Descartes, 67084 Strasbourg cedex, France

^b Laboratory of Experimental Rock Mechanics, École Polytechnique Fédérale de Lausanne, Station 18, CH-1015, Lausanne, Switzerland

^c Earth and Environmental Sciences, Ludwig-Maximilians-Universität, Theresienstr. 41, 80333 Munich, Germany

ARTICLE INFO

Article history:

Received 20 August 2016

Received in revised form 12 January 2017

Accepted 20 January 2017

Available online xxxx

Editor: J. Brodholt

Keywords:

compaction

andesite

porosity

conduit

permeability

outgassing

ABSTRACT

Explosive silicic volcanism is driven by gas overpressure in systems that are inefficient at outgassing. The zone at the margin of a volcanic conduit—thought to play an important role in the outgassing of magma and therefore pore pressure changes and explosivity—is the boundary through which heat is exchanged from the hot magma to the colder country rock. Using a simple heat transfer model, we first show that the isotherm for the glass transition temperature (whereat the glass within the groundmass transitions from a glass to an undercooled liquid) moves into the country rock when the magma within the conduit can stay hot, or into the conduit when the magma is quasi-stagnant and cools (on the centimetric scale over days to months). We then explore the influence of a migrating viscous boundary on compactive deformation micromechanisms in the conduit margin zone using high-pressure (effective pressure of 40 MPa), high-temperature (up to 800 °C) triaxial deformation experiments on porous andesite. Our experiments show that the micromechanism facilitating compaction in andesite is localised cataclastic pore collapse at all temperatures below the glass transition of the amorphous groundmass glass T_g (i.e., rock). In this regime, porosity is only reduced within the bands of crushed pores; the porosity outside the bands remains unchanged. Further, the strength of andesite is a positive function of temperature below the threshold T_g due to thermal expansion driven microcrack closure. The micromechanism driving compaction above T_g (i.e., magma) is the distributed viscous flow of the melt phase. In this regime, porosity loss is distributed and is accommodated by the widespread flattening and closure of pores. We find that viscous flow is much more efficient at reducing porosity than cataclastic pore collapse, and that it requires stresses much lower than those required to form bands of crushed pores. Our study therefore highlights that temperature excursions can result in a change in deformation micromechanism that drastically alters the mechanical and hydraulic properties of the material within the conduit margin zone, with possible implications for pore pressure augmentation and explosive behaviour.

© 2017 Elsevier B.V. All rights reserved.

1. Introduction

Magma vesiculation is the consequence of volatile oversaturation during decompression (Gonnermann and Manga, 2012) or heating (Lavallée et al., 2015). Once exsolved, the ease with which these volatiles can escape, governed by the permeability of the system, is thought to impact volcanic explosivity (Eichelberger et al., 1986; Woods and Koyaguchi, 1994; Melnik et al., 2005; Mueller et al., 2008). The conduit margin zone (comprising the magma at the conduit margin and the adjacent wall rock) is

thought to be the annulus through which degassed volatiles dominantly escape, a result of its highly fractured, brecciated, and banded nature (Rust et al., 2004; Tuffen and Dingwell, 2005; Lavallée et al., 2013; Gaunt et al., 2014).

The fractured physical state of the conduit margin zone is a consequence of the shear stresses in the magma-filled conduit (e.g., Tuffen and Dingwell, 2005). In the shallow edifice, a brittle response to an applied stress can be expected from (1) country rock adjacent to the conduit (Heap et al., 2015a), (2) volcanic material at the conduit margin without a substantial melt phase (i.e., high-crystallinity; Smith et al., 2011; Violay et al., 2012), and (3) magma with a substantial melt phase at the conduit margin deforming at a strain rate that exceeds the structural re-

* Corresponding author.

E-mail address: heap@unistra.fr (M.J. Heap).

laxation timescale of its melt phase (Ichihara and Rubin, 2010; Lavallée et al., 2013). Brittle deformation (i.e., fracture formation) increases the porosity and permeability of volcanic materials (Nara et al., 2011; Lavallée et al., 2013; Violay et al., 2015; Heap and Kennedy, 2016; Farquharson et al., 2016a), thus locally increasing the efficiency of outgassing and potentially decreasing the likelihood or intensity of an explosive eruption (Mueller et al., 2008; Lavallée et al., 2013; Castro et al., 2014).

Deeper in the edifice (≥ 1 km), the country rock adjacent to the conduit will accommodate stresses in a dominantly ductile manner (Shimada, 1986; Loaiza et al., 2012; Adelinet et al., 2013; Heap et al., 2015a). Ductile deformation in both the solid and liquid regimes can decrease the porosity, and therefore permeability, of the materials within the conduit margin zone, thus potentially increasing the likelihood or intensity of an explosive eruption (Kennedy et al., 2010; Kendrick et al., 2013; Heap et al., 2015a, 2015b; Schaubroth et al., 2016). The micromechanical mechanism responsible for ductile deformation in volcanic rocks (or magmas without a substantial melt phase) is distributed (Shimada, 1986; Zhu et al., 2011) or localised (Loaiza et al., 2012; Adelinet et al., 2013; Heap et al., 2015a) cataclastic pore collapse. Viscous flow of the amorphous melt phase is the mechanism responsible for ductile deformation in magma containing a substantial melt phase residing at a temperature above its glass transition temperature T_g (Quane et al., 2009; Lavallée et al., 2013; Kendrick et al., 2013; Vasseur et al., 2013; Heap et al., 2015b). We note that high strain rates can shift the transition from ductile to brittle deformation to greater depths (Webb and Dingwell, 1990; Cordonnier et al., 2012; Lavallée et al., 2013; Kushnir et al., 2017).

The zone at the margin of a volcanic conduit is the boundary through which heat is exchanged from the hot magma to the colder country rock. Temperature excursions, resulting from the injection of hot magma batches or the cooling of the magma within the conduit, will move the T_g isotherm thus modifying the operative micromechanism of deformation, with attendant implications for the mechanical response and the physical property evolution (e.g., porosity and permeability) of the materials within the margin zone. At a depth ≥ 1 km, where ductile deformation will dominate, the materials within the margin zone may repeatedly transition between the micromechanisms of cataclastic pore collapse and viscous flow. The transition between these compaction micromechanisms, and the accompanying changes in mechanical and hydraulic behaviour, has never been explicitly studied. Experimental studies of compaction in magmas have largely been limited to uniaxial experiments (Quane et al., 2009; Kendrick et al., 2013; Heap et al., 2014a) or isobaric conditions in which other forces, such as surface tension, dominate (Vasseur et al., 2013; Kennedy et al., 2015), while deformation experiments designed to study compaction in volcanic rocks have all been performed at ambient-temperature (Loaiza et al., 2012; Adelinet et al., 2013; Heap et al., 2015a). High-pressure and high-temperature studies of magma deformation have focussed on magma viscosity determination (e.g., Champallier et al., 2008) or the onset of fracturing (e.g., Kushnir et al., 2017) and, so far, have not provided *in-situ* measurements of porosity during deformation. A recent study however has shown, by means of a pore fluid volumeter, that compactive behaviour is encountered in low-porosity basalt at a confining pressure of 100 MPa and a temperature of 950 °C (Violay et al., 2015).

Our aim here is to investigate compaction processes in the conduit margin zone of a typical andesitic stratovolcano as the materials are heated or cooled. To achieve this goal we performed a series of high-pressure (at a pressure analogous to ~ 1 km depth) triaxial experiments on porous andesite at temperatures from ambient to 800 °C in which we monitored sample porosity during deformation. A detailed understanding of the micromechanical processes

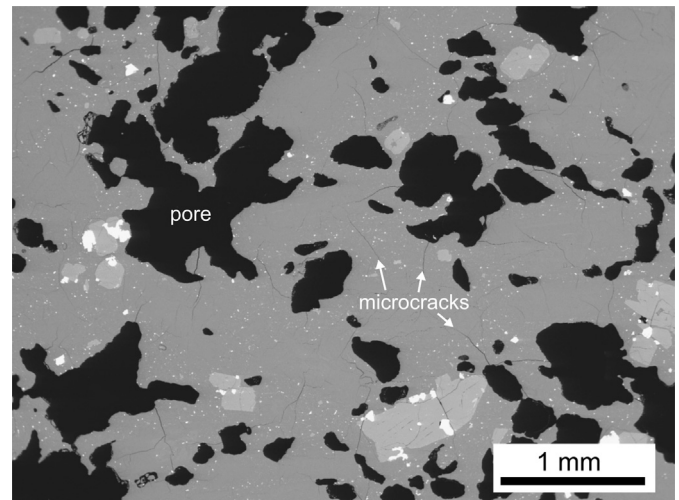


Fig. 1. Backscattered scanning electron microscope (BSEM) image of the as-collected andesite studied herein. Porosity is black. A pore and microcracks are labelled on the image.

responsible for compaction in the conduit margin zone, and how they influence mechanical behaviour and hydraulic properties, is paramount to our comprehension of pore pressure changes and the likelihood of explosive behaviour at active volcanoes worldwide.

2. Experimental material

We use an andesite block collected from the La Lumbre debris-flow track at Volcán de Colima, an active stratovolcano located in the Trans-Mexican Volcanic Belt (Mexico) (Varley and Komorowski, 2017). Although our block was sourced from Volcán de Colima, we consider the implications presented in this study to be applicable to active and frequently collapsing andesitic stratovolcanoes worldwide. Cylindrical core samples used for this study were all drilled from this block in the same orientation.

The andesite collected has a porphyritic texture consisting of a glassy groundmass (with abundant microlites) that hosts pores and a phenocryst cargo (long axis < 1.5 mm; Fig. 1). The phenocrysts and groundmass contain many randomly orientated microcracks up to a few mm in length (Fig. 1). The average connected and total porosity is 0.265 and 0.268 (isolated porosity ~ 0.03), respectively (determined by helium pycnometry; the connected porosity of each sample is given in Table 1). The phenocryst volume fraction is ~ 0.4 and the groundmass consists of glass (volume fraction ~ 0.135) containing ~ 0.2 volume fraction of microlites (of mainly plagioclase with subordinate high-density Fe–Ti oxides), estimated from 2D scanning electron microscope (SEM) images using ImageJ. The bulk composition of the here-studied andesite includes 61.5 wt.% SiO_2 , measured using X-ray fluorescence (XRF; complete XRF analysis is presented in the Supplementary Information), and is very similar to that of the products erupted over the last two decades (Heap et al., 2014b).

The temperature at which the glass within the groundmass transitions from a glass to an undercooled liquid—the glass transition temperature (T_g)—was determined using a Netzsch Pegasus 404 simultaneous thermal analysis device at a heating rate of $20^\circ\text{C min}^{-1}$. The glass transition is manifest as a non-linear endothermic peak in heat flow relative to the smoothly changing baseline value. During heating from the unknown natural cooling path during which the rock was formed, this peak occurred at $\sim 750.2 \pm 3.5^\circ\text{C}$ (see Supplementary Information for further details).

Table 1
Summary of the experiments performed for this study.

Connected porosity	Confining pressure (MPa)	Pore fluid pressure (MPa)	Pore fluid	Effective pressure (MPa)	Temperature (°C)	Strain rate (s ⁻¹)	Failure mode	Dominant deformation micromechanism
0.278	25	20	Water	5	Ambient	10 ⁻⁵	Brittle	Microcracking
0.267	30	20	Water	10	Ambient	10 ⁻⁵	Brittle	Microcracking
0.268	40	20	Water	20	Ambient	10 ⁻⁵	Brittle	Microcracking
0.269	50	20	Water	30	Ambient	10 ⁻⁵	Ductile	Cataclastic pore collapse
0.274	60	20	Water	40	Ambient	10 ⁻⁵	Ductile	Cataclastic pore collapse
0.275	70	20	Water	50	Ambient	10 ⁻⁵	Ductile	Cataclastic pore collapse
0.291	50	20	Argon	30	200	10 ⁻⁵	Ductile	Cataclastic pore collapse
0.248	50	20	Argon	30	400	10 ⁻⁵	Ductile	Cataclastic pore collapse
0.294	50	20	Argon	30	600	10 ⁻⁵	Ductile	Cataclastic pore collapse
0.281	50	20	Argon	30	800	10 ⁻⁵	Ductile	Viscous flow

3. Modelling

We will now consider whether, and to what extent, the spatial position of T_g will move with respect to the conduit margin. To do this, we apply a simple conductive solution to the 1D heat equation in cylindrical coordinates. We explore two end-member scenarios. First, where the magma remains at the initial maximum temperature and heat continuously conducts toward the far-field into the country rock. And second, where the magma in the conduit is stagnant and loses heat conductively into the country rock, leading to wholesale cooling of the system. While simplistic, to a first order the former scenario may be analogous to rapidly ascending magma (rapid advection end-member) while the latter may be analogous to very slowly ascending or stagnant conduit magma (no advection end-member). The 1D heat equation in cylindrical coordinates is:

$$\frac{\partial T}{\partial t} = \frac{1}{r} \frac{\partial}{\partial r} \left(r D \frac{\partial T}{\partial r} \right), \quad (1)$$

where r is the radial coordinate distance, t is the time since the onset of heat transfer, R is the conduit cylindrical radius, T is the temperature, and D is the thermal diffusivity. In both end-member cases we have the same initial conditions that are $T = T_m$ for $r \leq R$ at $t = 0$ and $T = T_r$ at $R \leq r \leq L$, where T_m and T_r are the initial temperature of the magma and the country rock, respectively. We take $T_m = 940^\circ\text{C}$ (estimated magmatic temperature for Volcán de Colima; Luhr and Carmichael, 1980) and $T_r = 50^\circ\text{C}$. We assume a first order estimate for the dependence of the thermal diffusivity D on temperature T is $D = D_0 \exp(\beta T)$, where D_0 is the diffusivity at $T = 0$ (in units of $^\circ\text{C}$) and β is a constant (after Schueroth et al., 2016). Following Schueroth et al. (2016), we compare the exponential form for D with the experimental data of Bagdassarov and Dingwell (1994) for pore-free volcanic material over the range of $550 \leq T \leq 1100^\circ\text{C}$. In this range we find that best fit values are $D_0 = 2.89 \times 10^{-7} \text{ m}^2 \text{ s}^{-1}$ and $\beta = 1.58 \times 10^{-3} \text{ }^\circ\text{C}^{-1}$. In the case where the magma and country rock are porous, we scale the effect of porosity by decomposing D into $D = k/\rho C$, the first-order scaling for porosity is then as follows:

$$D' = \frac{k(1 - \phi)}{(\rho C(1 - \phi) + \rho_f C_f \phi)(1 + \phi)} \quad (2)$$

where D' is the value of D scaled for ϕ , k is the pore-free thermal conductivity, ρ is the pore-free density, C is the pore-free specific heat capacity, ρ_f is the density of the pore fluid, C_f is the specific heat capacity of the pore fluid, and ϕ is the porosity. The bulk value of k is taken to be $D\rho C$ of the pore-free material. When $\phi = 0$, we then have the desirable limit that $D' = D$. Herein we take approximate values $\rho = 2000 \text{ kg m}^{-3}$, $C = 1000 \text{ J kg}^{-1} \text{ K}^{-1}$, $\rho_f = 1.275 \text{ kg m}^{-3}$, and $C_f = 1007 \text{ J kg}^{-1} \text{ K}^{-1}$. For a case where we invoke porosity, we replace D in Equation (1) with D' from Equation (2).

In our simulations of heat transfer, the conduit centre is insulated in both scenarios (Neumann boundary condition of 0) such that $\partial T/\partial r = 0$ for all t at $r/R = 0$. In the case where the magma remains hot throughout, we additionally have that $T = T_m$ for all t at $r/R \leq 1$. The scenario in which the magma is effectively stagnant and can cool, there is no boundary condition at $r/R = 1$ as we assume the material either side of the conduit wall follows the same $D(T)$ or $D'(T)$ law (see above). These assumptions are justified as the data from Bagdassarov and Dingwell (1994) show no discontinuity over this temperature range, even across T_g for any porosity. With these conditions, we solve Equation (1) numerically by using a fully implicit finite difference scheme (backward time, central space) coupled with a relaxed fixed-point method to ensure convergence at each time step, with a dimensionless spatial and temporal resolution of 10^{-3} and 10^{-4} , respectively. The results are shown in Fig. 2 for initial conduit radii of 15 and 50 m and initial country rock porosities of 0 and 0.4.

The model presented herein (Fig. 2) is a simplified numerical rendering of heat-transfer through conduit margin zones. In modelling conduction of heat from stagnant magma, repetitively injected magma, and continuously flowing magma to wall rocks, Petcovic and Dufek (2005) found that, for their conditions of a basaltic magma intruding a tonalitic wall rock, the amount of melting achieved in the wall rocks depended dominantly on the time since injection, the frequency of injection, and the time since the onset of continuous flow, in each case, respectively. Their model is composed of a coupled solution of the flow profile in the intrusion, the crystallisation and chemical mass transfer, and the heat transfer in both the magma and the wall rocks. Despite the complexity, a scaling between the time available for heat transfer t and the thermal diffusion length L holds such that $L \approx \sqrt{Dt}$, such that the half-fall distance of the temperature in published simulations scales with L until distances of ~ 10 m from the conduit. These authors use a temperature independent diffusivity of $D = 1.1 \times 10^{-6} \text{ m}^2 \text{ s}^{-1}$ so that this scaling is easily computed (see Supplementary Information). This simple scaling implies that L can be used to approximately predict heat transfer at the conduit boundary to a first order even for more complex conditions than the explicit solution given here (Fig. 2).

We find the intuitive result that T_g moves into the country rock in the case where the conduit magma does not cool (rapidly ascending magma), and that T_g moves into the conduit magma in the case where the conduit magma is quasi-stagnant and cools (Fig. 2). In the former case, the volume of material capable of viscous deformation will increase, enlarging the effective conduit radius (by 1–8 cm over days to months; Fig. 2a). These estimations are consistent with the observations of 0.1–2 cm-thick welded and densified rinds in the baked country rock at Tarawera volcano, New Zealand (Schueroth et al., 2016). Longer lengthscales (5–10 cm) of country rock viscous mobilisation will occur over timescales approaching a year (Fig. 2a). Conversely, in the latter case, cooling

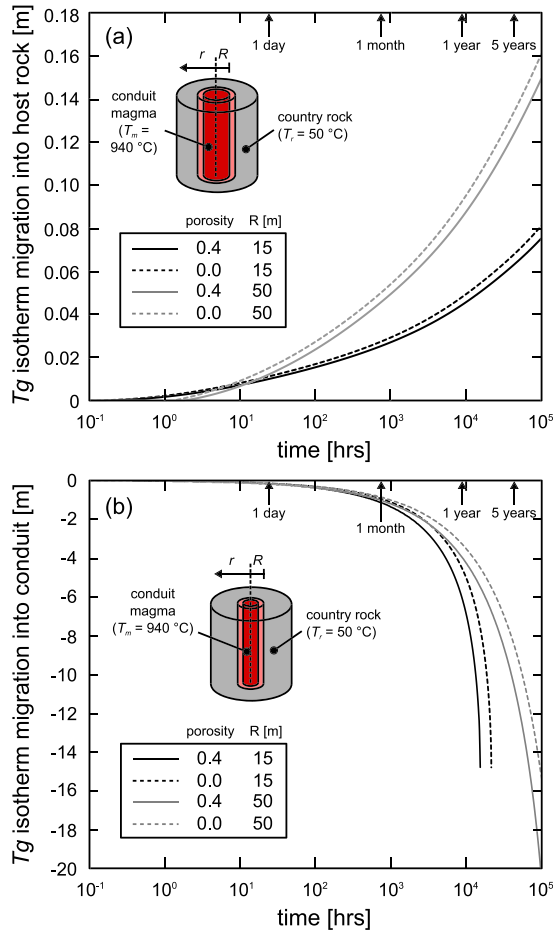


Fig. 2. The solution to the 1D heat equation in cylindrical coordinates for conductive heat transfer from a high-temperature magma-filled conduit ($T_m = 940^\circ\text{C}$) to the adjacent country rock ($T_r = 50^\circ\text{C}$). (a) Scenario in which the temperature of the magma is constant ($T = T_m$ for all t at $r/R \leq 1$). (b) Scenario in which the magma is allowed to cool (there is no boundary condition at $r/R = 1$). Curves are given for dense (porosity = 0) and porous (porosity = 0.4) country rock for two conduit radii, 15 and 50 m.

will result in a narrowing of the viscous radius of the magma conduit (by 15–100 cm over days to months; Fig. 2b). In this scenario, the viscous radius can be reduced by 4–5 m within one year (Fig. 2b).

It can be inferred from these models that the conduit margin zone—an important region of the edifice for magmatic outgassing—is subject to fluctuations in temperature that will modify the mechanical response and the physical property evolution (e.g., porosity and permeability) of the materials within the zone. We will now explore the influence of a migrating viscous deformation front on compactive deformation micromechanisms in the conduit margin zone using high-pressure and high-temperature triaxial deformation experiments.

4. Experimental considerations

Since our goal is to perform experiments at high-temperature, it is important to first understand whether exposure to high-temperature alters the physical state of the andesite (e.g., thermal microcracking). To this end, we measured the connected porosity, P-wave velocity, and permeability of two cylindrical samples (20 mm in diameter and precision-ground to a nominal length of 40 mm) at ambient temperature and after exposure to temperatures between 200 and 900°C . The samples were heated in a furnace at room pressure at a rate of 1°C min^{-1} and $20^\circ\text{C min}^{-1}$,

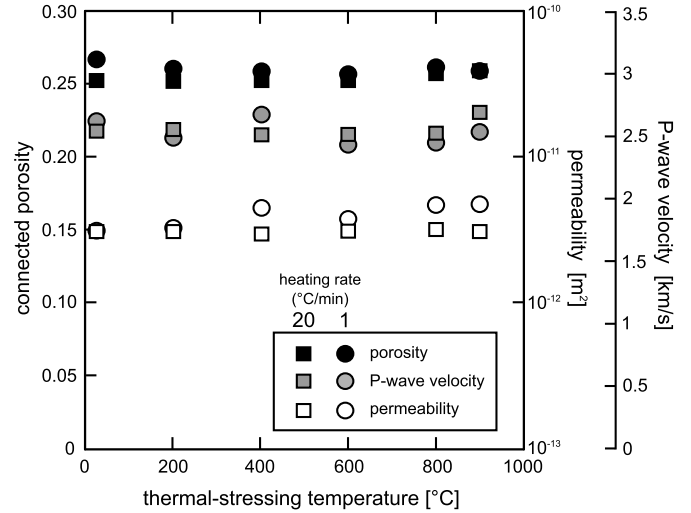


Fig. 3. Rock physical property evolution (connected porosity, permeability, and P-wave velocity) as a function of thermal stressing temperature (at two heating/cooling rates, 1 and $20^\circ\text{C min}^{-1}$).

respectively, left at the target temperature for 2 h, before being cooled back to room temperature at 1°C min^{-1} and $20^\circ\text{C min}^{-1}$, respectively. Connected porosity was measured using a helium pycnometer. P-wave velocity was measured along the axis of the sample under an axial stress of ~ 1 MPa. Permeability was measured along the sample axis in a steady-state gas (nitrogen) permeameter under a confining pressure P_c of 1 MPa (see the Supplementary Information for further details).

Our physical property data show that connected porosity, P-wave velocity, and permeability do not change upon transient (2 h) exposure to high-temperature (Fig. 3). Negligible changes to volcanic rock physical properties following thermal stressing has been previously noted in basalt heated to 900°C (Vinciguerra et al., 2005) and andesite heated to 450°C (Heap et al., 2014b). The absence of additional thermal microcracks in these thermally stressed samples was attributed to their high pre-existing microcrack density (Vinciguerra et al., 2005; Heap et al., 2014b), an observation that holds true for the andesite used herein (Fig. 1). Since rock physical properties are unaffected by thermal stressing (Fig. 3), the *in-situ* changes in mechanical behaviour can be wholly attributed to the *in-situ* pressure and temperature conditions, rather than changes to the physical state of the samples during heating to the target experimental temperature.

5. Experiments

5.1. Experimental methods

5.1.1. Ambient-temperature triaxial experiments

The focus of this study is to investigate ductile compactive micromechanisms in the conduit margin zone. To guide the effective pressure P_{eff} to be used in the high-temperature triaxial experiments, we first performed a suite of ambient-temperature triaxial deformation experiments ($\sigma_1 > \sigma_2 = \sigma_3$) to assess the pressure conditions under which the andesite is brittle and under which andesite is ductile (see 5.2.1 for a description of material failure modes). We assume here a simple effective pressure law of $P_{eff} = P_c - \alpha P_p$, where P_p is the pore fluid pressure. Here, the poroelastic constant α is taken to be unity, an assumption that is validated by a recent study in which this is explored for porous andesite (Farquharson et al., 2016b). We treat compressive stresses and strains as positive.

For the ambient-temperature triaxial experiments, cylindrical samples (20 mm in diameter and precision-ground to a nomi-

nal length of 40 mm) were prepared and vacuum saturated in deionised water. The samples were deformed at a range of P_c (confining fluid used was kerosene) at a constant P_p of 20 MPa (pore fluid used was deionised water). Samples were deformed in compression at a constant axial strain rate of 10^{-5} s^{-1} . Sample drainage at this strain rate was assured by their high permeability of $\sim 10^{-12} \text{ m}^2$ (fluid flow timescale is much shorter than the deformation timescale; see Heap and Wadsworth, 2016). A load cell and an LVDT recorded axial force and axial displacement, respectively, and a pore pressure intensifier monitored pore volume changes. These measurements were then converted to axial stress, axial strain, and connected porosity change using the sample dimensions. The deformation of the load train was removed from the measured axial displacement.

5.1.2. High-temperature triaxial experiments

For the high-temperature experiments, cylindrical samples 15 mm in diameter and precision-ground to between 33–36 mm in length were prepared and oven-dried at 70 °C for at least 48 h. Argon was used for the confining and pore fluid. Experiments were performed at temperatures between 200 and 800 °C and at a constant P_p of 20 MPa. Samples were heated at $\sim 20^\circ\text{C min}^{-1}$ to the target experimental temperature and, following deformation, cooled at the same rate. Copper jackets were used at temperatures $\leq 400^\circ\text{C}$; iron jackets were used for the experiments $\geq 600^\circ\text{C}$. Two iron jackets were used for the experiment performed at 800 °C to avoid a leak due to the substantial volumetric decrease of the sample. The contribution of the jacket strength was removed from the measured force using the estimates provided by Frost and Ashby (1982). Surface pores were filled with hardened ceramic paste to prevent jacket puncture. All samples were deformed in compression at an axial strain rate of 10^{-5} s^{-1} . An internal load cell and an LVDT recorded axial force and axial displacement, respectively, and a pore fluid volumeter monitored pore volume change. The difference between the temperature of the sample and that of the volumeter was accounted for by multiplying the ratio of the molar volumes of argon at both temperatures (ratios derived from Fischer and Paterson, 1989). These measurements were then converted to axial stress, axial strain, and connected porosity change using the sample dimensions. The deformation of the load train was removed from the measured axial displacement. A schematic of the high-temperature triaxial deformation apparatus can be found in Violay et al. (2015).

5.2. Experimental results

5.2.1. Ambient-temperature triaxial experiments

The relationship between increasing stress and increasing strain, and the evolution of connected porosity with strain for the ambient-temperature triaxial experiments ($5 < P_{eff} < 50 \text{ MPa}$) are presented in Fig. 4. The terms brittle and ductile are used here to describe the failure mode on the sample lengthscale. A brittle experiment involves an increase in porosity or decrease in the rate of compaction (dilatational microcracking) as strain increases towards macroscopic failure (grey curves in Fig. 4b) and strain softening (stress drop) following a peak stress (grey curves in Fig. 4a). A brittle failure mode is confirmed by the presence of a shear fracture preserved in the sample after the experiment. We use here the definition of ductility provided by Rutter (1986): the capacity of a material to deform to a substantial strain without the tendency to localise the deformation into faults (although there are instances of compaction localisation in the ductile domain, see Heap et al., 2015a). The concept of ductility, as interpreted by Rutter (1986) and herein, is not dependent on the deformation micromechanism. Ductile experiments are purely compactional (grey curves in Fig. 4b). From these data (Fig. 4) we conclude that the andesite

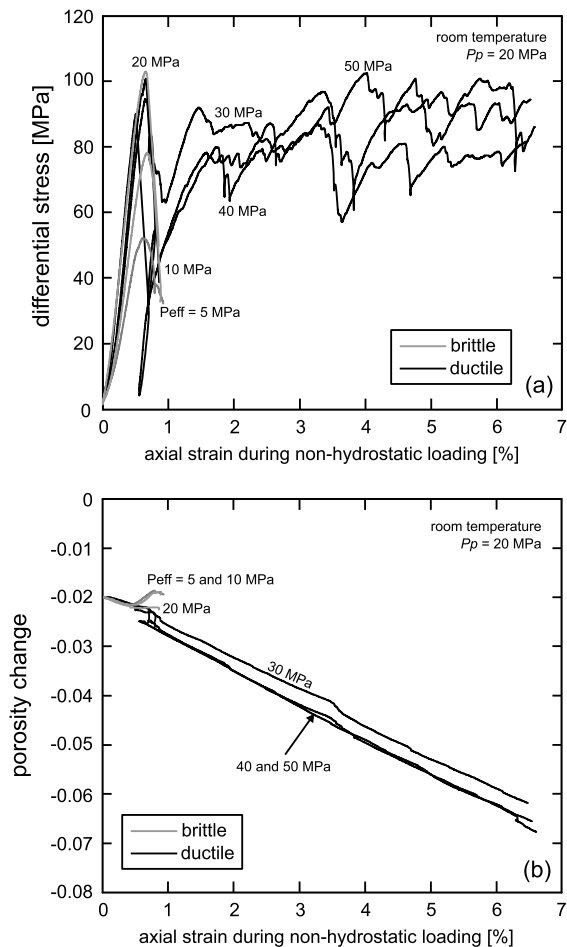


Fig. 4. Ambient-temperature triaxial experiments. (a) Ambient-temperature stress–strain curves for andesite samples deformed at a range of effective pressures (P_{eff} ; the experimental pressure is indicated next to each curve). (b) Connected porosity change as a function of axial strain for the experiments shown in panel (a). The connected porosity decrease during the hydrostatic portion of the experiment (i.e., prior to differential stressing) was subtracted from each curve. Brittle curves are shown in grey and ductile curves are shown in black.

is brittle at $5 < P_{eff} < 20 \text{ MPa}$ and ductile at $P_{eff} > 30 \text{ MPa}$. In the brittle regime, the peak stress increases as P_c is increased from 5 to 20 MPa (black curves in Fig. 4a). The evolution of stress with increasing strain in the ductile regime is characterised by small stress drops (black curves in Fig. 4a); stress drops during compactant behaviour in volcanic rocks have been previously attributed to compaction localisation (Heap et al., 2015a). Since our interest here is compaction, we used $P_{eff} = 40 \text{ MPa}$ ($P_c = 60 \text{ MPa}$; $P_p = 20 \text{ MPa}$) for our high-temperature deformation experiments.

5.2.2. High-temperature triaxial experiments

The stress–strain curves and connected porosity reduction curves for the high-temperature (up to 800 °C) triaxial experiments ($P_{eff} = 40 \text{ MPa}$) are presented in Fig. 5. The stress–strain curves at temperatures between 200 and 600 °C (i.e., below T_g on the timescale of the experiment) are qualitatively similar to those at ambient-temperature (Fig. 4a) in that many small stress drops are observed (Fig. 5a). We also note that the samples deformed at temperatures between 200 and 600 °C are stiffer than the ambient-temperature sample, and that the differential stress before the first stress drop increases as temperature increases, from $\sim 90 \text{ MPa}$ at ambient-temperature to $\sim 200 \text{ MPa}$ at 600 °C (Fig. 5a). The mechanical behaviour is markedly different for the sample deformed at 800 °C (Fig. 5). The sample is considerably weaker and shows strain hardening up to the maximum axial

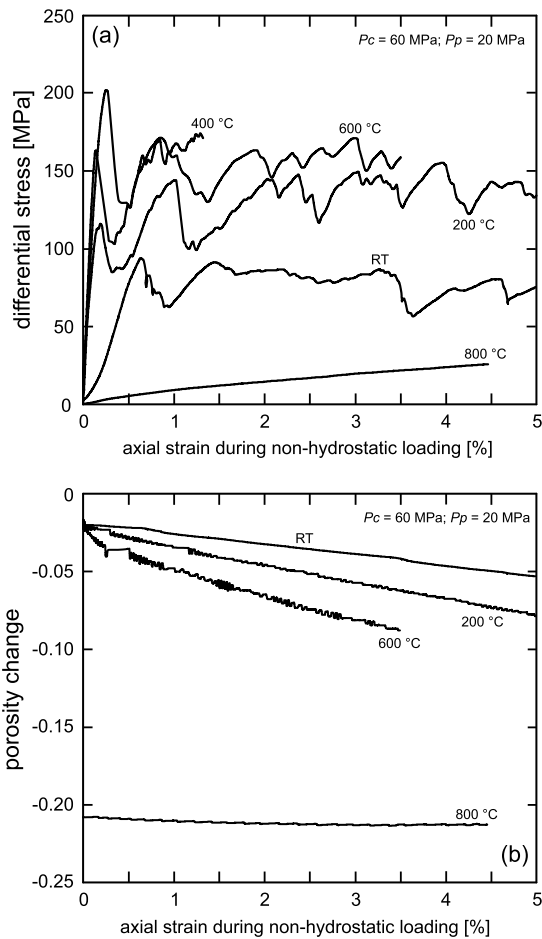


Fig. 5. High-temperature triaxial experiments. (a) Stress–strain curves for andesite samples deformed at a range of temperatures (ambient-temperature to 800 °C; the experimental temperature is indicated next to each curve) at $P_{eff} = 40$ MPa. (b) Connected porosity change as a function of axial strain for the experiments shown in panel (a). Connected porosity change was not monitored during the hydrostatic portion of the high-temperature experiments. Hydrostatic connected porosity change for the tests performed below T_g was assumed to be the same as those performed at ambient-temperature (porosity reduction of 0.02). Hydrostatic porosity change for the 800 °C sample was estimated using the initial porosity of the sample, the 2D porosity of the sample following deformation (determined using ImageJ), and the connected porosity change measured *in-situ* during deformation.

strain of 4.5% (Fig. 5a). Porosity decreased from the initial 0.265 to 0.065 during the hydrostatic portion of the experiment (estimated from the 2D porosity determined from a post-deformation SEM photomicrograph minus the connected porosity change measured during the experiment). During deformation at constant strain rate, the connected porosity decreased by a further ~ 0.05 at the maximum axial strain of 4.5% (Fig. 5b).

6. Discussion

6.1. Strengthening of andesite below T_g

Our mechanical data show that there is a progressive strengthening as temperature is increased below the threshold T_g (Fig. 5a). For example, the differential stress before the first stress drop at 600 °C is more than twice that at ambient-temperature (Fig. 5a). We interpret this strengthening as a consequence of the closure of pre-existing microcracks (abundant in this material; Fig. 1) due to the thermal expansion of the mineral assemblage. Previous studies have reported an increase in the strength of volcanic rock at high temperature. For example, Meredith and Atkinson (1985) measured an increase in fracture toughness in gabbro from ambient-

temperature to 100 °C and Duclos and Paquet (1991) reported an increase in the compressive strength of basalt, from ~ 340 MPa at ambient-temperature to ~ 450 MPa at 650 °C. We note that the strengthening of the samples as temperature is increased in the regime below T_g may be reduced at strain rates lower than 10^{-5} s^{-1} due to temperature-sensitive subcritical crack growth processes such as stress corrosion (Brantut et al., 2013).

6.2. Micromechanical mechanisms of compaction

The micromechanism driving the compaction in the samples deformed at ambient-temperature and up to 600 °C (i.e., below T_g) is cataclastic pore collapse (Fig. 6a). The compaction is localised into bands (~ 2 mm in width) orientated subperpendicular to the maximum principal stress; these bands of crushed pores are similar to those observed in previously published ambient-temperature experiments (Loaiza et al., 2012; Adelinet et al., 2013; Heap et al., 2015a). The experiments reported here are the first to document localised pore collapse in volcanic rocks at temperatures greater than ambient. The porosity within the band is ~ 0.12 (measured on 2D SEM images using ImageJ). Due to the localised nature of the deformation, the porosity is largely unchanged outside of the band (porosity ≈ 0.26). Contrastingly, the micromechanism facilitating compaction at 800 °C (i.e., above T_g) was distributed viscous flow of the melt phase (Fig. 6b). Substantial porosity loss is the result of the flattening and closing of connected pores (Fig. 6b), as previously documented in uniaxial (Quane et al., 2009; Kendrick et al., 2013) and isobaric (Vasseur et al., 2013; Kennedy et al., 2015) experiments. We observe no significant change to the crystal cargo, and no preferred orientation for the crystals and flattened pores (Fig. 6b). We note that isolated pores may deform under applied shear stresses (e.g., Llewellyn et al., 2002), shrink slightly at high pressures (e.g., Proussevitch et al., 1993), or resorb, if the volatile phase is soluble in the melt (e.g., McIntosh et al., 2014), but will not compact in the same way as connected pores. Herein, the porosity change we measure during deformation is that of the interconnected pore space that can readily outgas the pore fluid phase and close shut as a result.

6.3. Volcanological significance

The conduit margin zone is thought to assist magmatic outgassing (Rust et al., 2004; Tuffen and Dingwell, 2005; Lavallée et al., 2013; Gaunt et al., 2014; Farquharson et al., 2016c; Kendrick et al., 2016), a key factor for the dissipation of pore pressure and therefore the cessation of explosive behaviour. This zone will be subject to fluctuations in temperature as heat is transferred from the hot, conduit-dwelling magma to the colder country rock. At a depth ≥ 1 km, the migration of the T_g isotherm (Fig. 2) in the conduit margin zone will promote a change in compaction deformation micromechanism (Fig. 6) that drastically influences strength and porosity loss during compaction (Fig. 5).

Material below T_g will accommodate small stresses elastically, while larger stress perturbations will result in the formation of bands of crushed pores (Fig. 6a). Such bands—that are of lower porosity than the rock in which they are hosted—have been previously shown to reduce permeability by up to an order of magnitude in porous andesite (initial connected porosity ≈ 0.19 ; Heap et al., 2015a). If the differential stress imposed on the conduit margin zone is subperpendicular to the conduit wall, we would expect these features to be orientated parallel to the conduit margin (Fig. 7). Bands of crushed pores that form in the conduit margin zone are thus expected to impede the outgassing of the nearby magma-filled conduit, although it is at present unclear whether such features can form a coherent low-permeability barrier.

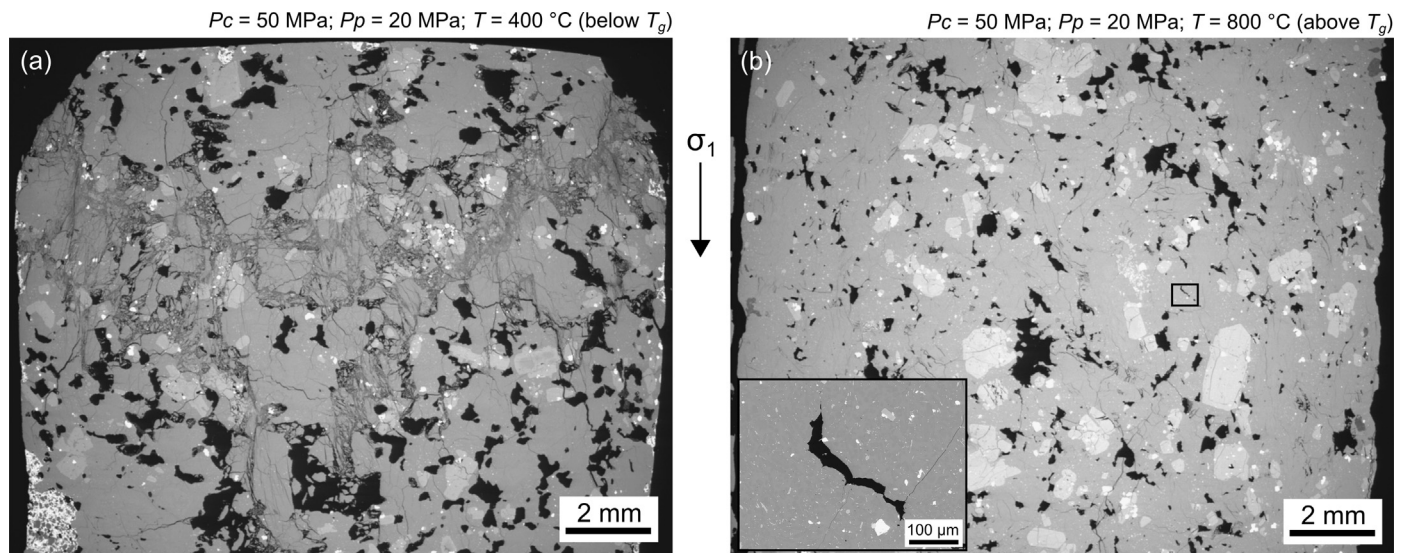


Fig. 6. Ductile deformation microstructures below and above T_g . (a) Backscattered scanning electron microscope (BSEM) image of the sample deformed at 400 °C ($P_{eff} = 40$ MPa) showing the band of crushed pores (running across the diameter of the sample). (b) BSEM image of the sample deformed at 800 °C ($P_{eff} = 40$ MPa) showing distributed viscous compaction. Inset shows a viscously flattened pore.

Material above T_g will accommodate stress through viscous flow (Fig. 6b). The change in micromechanism from cataclastic pore collapse to viscous flow is accompanied by a significant reduction to the strength (Fig. 5a) and a substantial and distributed loss of porosity as pores are flattened and closed (Fig. 6b). Since a porosity loss from ~ 0.256 to ~ 0.06 is likely to reduce permeability by four orders of magnitude (Farquharson et al., 2015), the migration of the T_g isotherm into the country rock (increasing the effective conduit radius) will significantly lower permeability of the conduit margin zone (Fig. 7a). The reduction in porosity and permeability is expected to inhibit the outgassing of the nearby magma-filled conduit, leading to the preservation of high overpressures and thus increasing the probability of explosive behaviour (Kennedy et al., 2010; Schaubroth et al., 2016).

If magma is emplaced in the conduit and then remains stagnant for a period of time before the next episode of up-flow and emplacement (as explored by Petcovic and Dufek, 2005) or if the conduit ascent rate is variable (as suggested for Volcán de Colima by Cassidy et al., 2015), then the spatial position of the T_g isotherm is likely to fluctuate outward and inward with respect to an initial conduit margin. Such a spatially mobile T_g isotherm implies that parts of the conduit margin zone are likely repeatedly cycled above and below T_g . Due to the particle-size dependence of viscous sintering (e.g., Wadsworth et al., 2016), any bands of collapsed pores in a material taken above T_g will efficiently heal thus creating a band of very low porosity and permeability. Material compacted viscously—and therefore low-porosity—taken below T_g will likely respond in a brittle manner to an applied stress, due to the porosity dependence of brittle versus ductile behaviour in volcanic rocks (Heap et al., 2015a). This cyclicity of deformation micromechanisms at the conduit margin has implications for the distribution of outgassing pathways that can be formed or destroyed in that zone (see the varied textures and overprinting textures presented in Tuffen and Dingwell, 2005 and Farquharson et al., 2016c, for example) and for the switch between seismogenic and aseismic periods of flow (Tuffen et al., 2003; Neuberg et al., 2006; Lavallée et al., 2008).

Fluctuations in the permeability of the conduit margin zone should now be considered in models of conduit outgassing (Collinson and Neuberg, 2012) and in the interpretation of outgassing fluctuations monitored at active volcanoes (Edmonds et al., 2003).

7. Conclusions

The conduit margin zone—defined as the country rock and the magma close to the conduit margin—is thought to be the annulus through which magmas outgas (e.g., Rust et al., 2004; Tuffen and Dingwell, 2005; Lavallée et al., 2013; Farquharson et al., 2016c; Kendrick et al., 2016). Therefore, a decrease of porosity and permeability for the material within this zone could impede outgassing and lead to pressure build-up and explosive behaviour. Since the conduit margin zone is the boundary through which heat is exchanged from the hot magma to the colder country rock, it is prone to fluctuations in temperature. A simple model of heat transfer shows that the T_g isotherm can move (on the centimetric scale over days to months) into the country rock when the magma within the conduit can stay hot, or move into the conduit when the magma is quasi-stagnant and cools.

Triaxial deformation experiments designed to explore the micromechanisms of compaction above and below T_g show that while ductile deformation below T_g is localised, manifest as bands of crushed pores oriented perpendicular to the maximum principal stress, ductile deformation above T_g is facilitated by distributed viscous flow. Our experiments show that viscous flow requires stresses much lower than those required to form bands of collapsed pores in volcanic rock, and that it is a much more efficient at reducing the porosity, and therefore permeability, of the materials within the conduit margin zone.

Our study therefore highlights that fluctuations in temperature can result in a change in deformation micromechanism that drastically alters the mechanical and hydraulic properties of the material within the conduit margin zone, with possible implications for pore pressure augmentation and explosive behaviour.

Acknowledgements

M.J.H. acknowledges funding from an Initiative d'Excellence (IDEX) "Attractivité" grant (VOLPERM), funded by the University of Strasbourg. M.V. acknowledges funding from EPFL. Nick Varley, Jamie Farquharson, and Oliver Lamb are thanked for field assistance. Gilles Morvan is thanked for SEM assistance. Luke Griffiths, Patrick Baud, Thierry Reuschlé, and Alexandra Kushnir are also warmly thanked. M.V. thanks Jean-Pierre Burg and Claudio Madonna for access to the laboratory at ETH Zürich. This work has

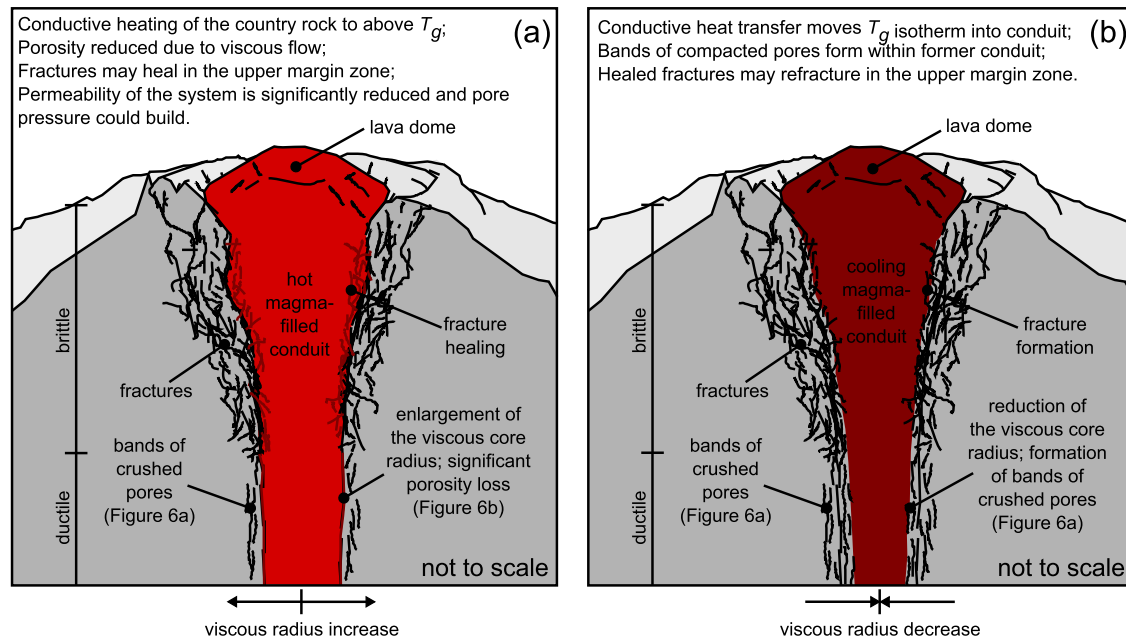


Fig. 7. Cartoons (not to scale) highlighting the salient implications of this study. (a) Country rock within the conduit margin zone is heated above T_g (e.g., rapidly ascending magma), expanding the effective conduit radius. Viscous compaction leads to a large reduction in porosity and permeability of the conduit margin zone, potentially reducing outgassing capability and augmenting pore pressure. (b) Magma cools and the T_g isotherm retreats inside the conduit (e.g., slow-moving or stagnant magma), reducing the effective conduit radius. Stresses within the conduit margin zone may create bands of crushed pores (subparallel to the conduit margin) within the former conduit. Bands of crushed pores are expected to disrupt outgassing, although it is at present unclear whether such features can form a coherent low-permeability barrier.

benefited from Labex grant ANR-11-LABX-0050_G-EAU-THERMIE-PROFONDE and therefore benefits from state funding managed by the Agence Nationale de la Recherche (ANR) as part of the “Investissements d’avenir” program. The European Research Council advanced grant EVOKES (247076) provided funding for F.B.W. The authors acknowledge support from a Partenariats Hubert Curien (PHC) PROCOPE grant (grant number 332065SG). We thank Yan Lavallée and one anonymous reviewer for constructive comments that helped us improve this manuscript.

Appendix A. Supplementary material

Supplementary material related to this article can be found online at <http://dx.doi.org/10.1016/j.epsl.2017.01.021>.

References

- Adelinet, M., Fortin, J., Schubnel, A., Guéguen, Y., 2013. Deformation modes in an Icelandic basalt: from brittle failure to localized deformation bands. *J. Volcanol. Geotherm. Res.* 255, 12–25.
- Bagdasarov, N.S., Dingwell, D.B., 1994. Thermal properties of vesicular rhyolite. *J. Volcanol. Geotherm. Res.* 60, 179–191.
- Brantut, N., Heap, M.J., Meredith, P.G., Baud, P., 2013. Time-dependent cracking and brittle creep in crustal rocks: a review. *J. Struct. Geol.* 52, 17–43.
- Cassidy, M., Cole, P.D., Hicks, K.E., Varley, N.R., Peters, N., Lerner, A.H., 2015. Rapid and slow: varying magma ascent rates as a mechanism for Vulcanian explosions. *Earth Planet. Sci. Lett.* 420, 73–84.
- Castro, J., Bindeman, I.N., Tuffen, H., Schipper, C.I., 2014. Explosive origin of silicic lava: textural and $\delta D-H_2O$ evidence for pyroclastic degassing during rhyolite effusion. *Earth Planet. Sci. Lett.* 405, 52–61.
- Champallier, R., Bystricky, M., Arbaret, L., 2008. Experimental investigation of magma rheology at 300 MPa: from pure hydrous melt to 76 vol.% of crystals. *Earth Planet. Sci. Lett.* 267, 571–583.
- Collinson, A.S.D., Neuberg, J., 2012. Gas storage, transport and pressure changes in an evolving permeable volcanic edifice. *J. Volcanol. Geotherm. Res.* 243–244, 1–13.
- Cordonnier, B., Caricchi, L., Pistone, M., Castro, J., Hess, K.U., Gottschaller, S., Manga, M., Dingwell, D.B., Burlini, L., 2012. The viscous–brittle transition of crystal-bearing silicic melt: direct observation of magma rupture and healing. *Geology* 40 (7), 611–614.
- Duclos, R., Paquet, J., 1991. High-temperature behaviour of basalts—role of temperature and strain rate on compressive strength and K_{IC} toughness of partially glassy basalts at atmospheric pressure. *Int. J. Rock Mech. Min. Sci. Geomech. Abstr.* 28, 71–76.
- Edmonds, M., Herd, R.A., Galle, B., Oppenheimer, C.M., 2003. Automated, high time-resolution measurements of SO_2 flux at Soufrière Hills Volcano, Montserrat. *Bull. Volcanol.* 65, 578–586.
- Eichelberger, J.C., Carrigan, C.R., Westrich, H.R., Price, P.H., 1986. Non-explosive silicic volcanism. *Nature* 323, 598–602.
- Farquharson, I.J., Heap, M.J., Varley, N., Baud, P., Reuschlé, T., 2015. Permeability and porosity relationships of edifice-forming andesites: a combined field and laboratory study. *J. Volcanol. Geotherm. Res.* 297, 52–68.
- Farquharson, J.L., Heap, M.J., Baud, P., 2016a. Strain-induced permeability increase in volcanic rock. *Geophys. Res. Lett.* 43. <http://dx.doi.org/10.1002/2016GL071540>.
- Farquharson, J.L., Heap, M.J., Baud, P., Reuschlé, T., Varley, N., 2016b. Pore pressure embrittlement in a volcanic edifice. *Bull. Volcanol.* 78 (6).
- Farquharson, J.L., Heap, M.J., Lavallée, Y., Varley, N., Baud, P., 2016c. Evidence for the development of permeability anisotropy in lava domes and volcanic conduits. *J. Volcanol. Geotherm. Res.* 323, 163–185.
- Fischer, G.J., Paterson, M.S., 1989. Dilatancy during rock deformation at high temperatures and pressures. *J. Geophys. Res.* 94 (B12), 17607–17617.
- Frost, H.J., Ashby, M.F., 1982. *Deformation-Mechanism Maps*. Pergamon, Oxford.
- Gaunt, H.E., Sammonds, P.R., Meredith, P.G., Smith, R., Pallister, J.S., 2014. Pathways for degassing during the lava dome eruption of Mount St. Helens 2004–2008. *Geology* 42 (11), 947–950.
- Gonnermann, H.M., Manga, M., 2012. Dynamics of magma ascent in the volcanic conduit. In: Fagents, S.A., Gregg, T.K.P., Lopes, R.M.C. (Eds.), *Modeling Volcanic Processes: the Physics and Mathematics of Volcanism*. Cambridge University Press, Cambridge.
- Heap, M.J., Kolzenburg, S., Russell, J.K., Campbell, M.E., Welles, J., Farquharson, J.L., Ryan, A., 2014a. Conditions and timescales for welding block-and-ash flow deposits. *J. Volcanol. Geotherm. Res.* 289, 202–209.
- Heap, M.J., Lavallée, Y., Petrakova, L., Baud, P., Reuschlé, T., Varley, N.R., Dingwell, D.B., 2014b. Microstructural controls on the physical and mechanical properties of edifice-forming andesites at Volcán de Colima, Mexico. *J. Geophys. Res.* 119 (4), 2925–2963.
- Heap, M.J., Farquharson, I.J., Baud, P., Lavallée, Y., Reuschlé, T., 2015a. Fracture and compaction of andesite in a volcanic edifice. *Bull. Volcanol.* 77, 55. <http://dx.doi.org/10.1007/s00445-015-0938-7>.
- Heap, M.J., Farquharson, I.J., Wadsworth, F.B., Kolzenburg, S., Russell, J.K., 2015b. Timescales for permeability reduction and strength recovery in densifying magma. *Earth Planet. Sci. Lett.* 429, 223–233.
- Heap, M.J., Kennedy, B.M., 2016. Exploring the scale-dependent permeability of fractured andesite. *Earth Planet. Sci. Lett.* 447, 139–150.
- Heap, M.J., Wadsworth, F.B., 2016. Closing an open system: pore pressure changes in permeable edifice rock at high strain rates. *J. Volcanol. Geotherm. Res.* 315, 40–50.

- Ichihara, M., Rubin, M.B., 2010. Brittleness of fracture in flowing magma. *J. Geophys. Res.* 115. <http://dx.doi.org/10.1029/2010JB007820>.
- Kendrick, J.E., Lavallée, Y., Hess, K.-U., Heap, M.J., Gaunt, H.E., Meredith, P.G., Dingwell, D.B., 2013. Tracking the permeable porous network during strain-dependent magmatic flow. *J. Volcanol. Geotherm. Res.* 260, 117–126.
- Kendrick, J.E., Lavallée, Y., Varley, N.R., Wadsworth, F.B., Lamb, O.D., Vasseur, J., 2016. Blowing off stream: tuffsite formation as a regulator for lava dome eruptions. *Front. Earth Sci.* 4. <http://dx.doi.org/10.2289/feart.2016.00041>.
- Kennedy, B.M., Jellinek, A.M., Russell, J.K., Nichols, A.R.L., Vigouroux, N., 2010. Time- and temperature-dependent conduit wall porosity: a key control on degassing and explosivity at Tarawera volcano, New Zealand. *Earth Planet. Sci. Lett.* 299, 126–137.
- Kennedy, B.M., Wadsworth, F.B., Vasseur, J., Schipper, C.I., Jellinek, A.M., von Aulock, F.W., Hess, K.-U., Russell, J.K., Lavallée, Y., Nichols, A.R.L., Dingwell, D.B., 2015. Surface tension driven processes densify and retain permeability in magma and lava. *Earth Planet. Sci. Lett.* 433, 116–124.
- Kushnir, A.R., Martel, C., Champallier, R., Arbaret, L., 2017. In situ confirmation of permeability development in shearing bubble-bearing melts and implications for volcanic outgassing. *Earth Planet. Sci. Lett.* 458, 315–326.
- Lavallée, Y., Meredith, P.G., Dingwell, D.B., Hess, K.-U., Wassermann, J., Cordonnier, B., Gerik, A., Kruhl, J.H., 2008. Seismogenic lavas and explosive eruption forecasting. *Nature* 453, 507–510.
- Lavallée, Y., Benson, P.M., Heap, M.J., Hess, K.-U., Flaws, A., Schillinger, B., Meredith, P.G., Dingwell, D.B., 2013. Reconstructing magma failure and the degassing network of dome-building eruptions. *Geology* 41, 515–518.
- Lavallée, Y., Dingwell, D.B., Johnson, J.B., Cimarelli, C., Hornby, A.J., Kendrick, J.E., von Aulock, F.W., Kennedy, B.M., Andrews, B.J., Wadsworth, F.B., Rhodes, E., Chinga, G., 2015. Thermal vesiculation during volcanic eruptions. *Nature* 528, 544–547.
- Llewellyn, E.W., Mader, H.M., Wilson, S.D.R., 2002. The rheology of a bubbly liquid. *Proc. R. Soc. A* 458. <http://dx.doi.org/10.1098/rspa.2001.0924>.
- Loaiza, S., Fortin, J., Schubnel, A., Guéguen, Y., Vinciguerra, S., Moreira, M., 2012. Mechanical behavior and localized failure modes in a porous basalt from the Azores. *Geophys. Res. Lett.* 39. <http://dx.doi.org/10.1029/2012GL053218>.
- Luhr, J.F., Carmichael, I.S., 1980. The Colima volcanic complex, Mexico. *Contrib. Mineral. Petrol.* 71 (4), 343–372.
- McIntosh, I.M., Llewellyn, E.W., Humphreys, M.C.S., Nichols, A.R.L., Burgisser, A., Schipper, C.I., Larsen, J.F., 2014. Distribution of dissolved water in magmatic glass records growth and resorption of bubbles. *Earth Planet. Sci. Lett.* 401, 1–11.
- Melnik, O., Barmin, A.A., Sparks, R.S.J., 2005. Dynamics of magma flow inside volcanic conduits with bubble overpressure buildup and gas loss through permeable magma. *J. Volcanol. Geotherm. Res.* 142, 53–68.
- Meredith, P.G., Atkinson, B.K., 1985. Fracture toughness and subcritical crack growth during high-temperature tensile deformation of Westerly granite and Black gabbro. *Phys. Earth Planet. Inter.* 39, 33–51.
- Mueller, S., Scheu, B., Spieler, O., Dingwell, D.B., 2008. Permeability control on magma fragmentation. *Geology* 36, 399–402.
- Nara, Y., Meredith, P.G., Yoneda, T., Kaneko, K., 2011. Influence of macro-fractures and micro-fractures on permeability and elastic wave velocities in basalt at elevated pressure. *Tectonophysics* 503, 52–59.
- Neuberg, J.W., Tuffen, H., Collier, L., Green, D., Powell, T., Dingwell, D.B., 2006. The trigger mechanism of low-frequency earthquakes on Montserrat. *J. Volcanol. Geotherm. Res.* 153, 37–50.
- Petcovic, H.L., Dufek, J.D., 2005. Modeling magma flow and cooling in dikes: implications for emplacement of Columbia River flood basalts. *J. Geophys. Res.* 110. <http://dx.doi.org/10.1029/2004JB003432>.
- Proussevitch, A.A., Sahagian, D.L., Anderson, A.T., 1993. Dynamics of diffusive bubble growth in magmas: isothermal case. *J. Geophys. Res.* 98, 22283–22307.
- Quane, S.L., Russell, J.K., Friedlander, E.A., 2009. Time scales of compaction in volcanic systems. *Geology* 37, 471–474.
- Rust, A.C., Cashman, K.V., Wallace, P.J., 2004. Magma degassing buffered by vapor flow through brecciated conduit margins. *Geology* 32, 349–352.
- Rutter, E., 1986. On the nomenclature of mode of failure transitions in rocks. *Tectonophysics* 122, 381–387.
- Schairoth, J., Wadsworth, F.B., Kennedy, B.M., von Aulock, F.W., Lavallée, Y., Damby, D.E., Vasseur, J., Scheu, B., Dingwell, D.B., 2016. Conduit margin heating and deformation during the AD 1886 basaltic Plinian eruption at Tarawera volcano, New Zealand. *Bull. Volcanol.* 78 (2). <http://dx.doi.org/10.1007/s00445-016-1006-7>.
- Shimada, M., 1986. Mechanism of deformation in a dry porous basalt at high pressures. *Tectonophysics* 121, 153–173.
- Smith, R., Sammonds, P., Tuffen, H., Meredith, P.G., 2011. Evolution of the mechanics of the 2004–2008 Mt. St. Helens lava dome with time and temperature. *Earth Planet. Sci. Lett.* 307, 191–200.
- Tuffen, H., Dingwell, D.B., Pinkerton, H., 2003. Repeated fracture and healing of silicic magma generate flow banding and earthquakes? *Geology* 31, 1089–1092.
- Tuffen, H., Dingwell, D.B., 2005. Fault textures in volcanic conduits: evidence for seismic trigger mechanisms during silicic eruptions. *Bull. Volcanol.* 67, 370–387.
- Varley, N., Komorowski, J.-C., 2017. *Volcán de Colima: Managing the Threat*. Springer. ISBN 978-3-642-25911-1.
- Vasseur, J., Wadsworth, F.B., Lavallée, Y., Hess, K.-U., Dingwell, D.B., 2013. Volcanic sintering: timescales of viscous densification and strength recovery. *Geophys. Res. Lett.* 40, 5658–5664.
- Vinciguerra, S., Trovato, C., Meredith, P.G., Benson, P.M., 2005. Relating seismic velocities, thermal cracking and permeability in Mt. Etna and Iceland basalts. *Int. J. Rock Mech. Min. Sci.* 42, 900–910.
- Violay, M., Gibert, B., Mainprice, D., Evans, B., Dautria, J.-M., Azias, P., Pezard, P., 2012. An experimental study of the brittle–ductile transition of basalt at oceanic crust pressure and temperature conditions. *J. Geophys. Res.* 117 (B3). <http://dx.doi.org/10.1029/2011JB008884>.
- Violay, M., Gibert, B., Mainprice, D., Burg, J.-P., 2015. Brittle versus ductile deformation as the main control of the deep fluid circulation in oceanic crust. *Geophys. Res. Lett.* 42. <http://dx.doi.org/10.1002/2015GL063437>.
- Wadsworth, F.B., Vasseur, J., Llewellyn, E.W., Schairoth, J., Dobson, K.J., Scheu, B., Dingwell, D.B., 2016. Sintering of viscous droplets under surface tension. *Proc. R. Soc. A* 472. <http://dx.doi.org/10.1098/rspa.2015.0780>.
- Webb, S.L., Dingwell, D.B., 1990. The onset of non-Newtonian rheology of silicate melts—a fiber elongation study. *Phys. Chem. Mater.* 17, 125–132.
- Woods, A.W., Koyaguchi, T., 1994. Transitions between explosive and effusive eruptions of silicic magmas. *Nature* 370, 641–644.
- Zhu, W., Baud, P., Vinciguerra, S., Wong, T.-F., 2011. Micromechanics of brittle faulting and cataclastic flow in Alban Hills tuff. *J. Geophys. Res.* 116, B06209. <http://dx.doi.org/10.1029/2010JB008046>.